Interactive and Multi-modal Visualization for Neuroendoscopic Interventions

Dirk Bartz[1], Wolfgang Straßer[1], Özlem Gürvit[2,3],
Dirk Freudenstein[3], and Martin Skalej[2]

[1] WSI/GRIS, University of Tübingen,
Auf der Morgenstelle 10/C9,
D72076 Tübingen, Germany
Email: {bartz,strasser}@gris.uni-tuebingen.de
[2] Department of Neuroradiology,
[3] Department of Neurosurgery,
University Hospital Tübingen
Hoppe-Seyler-Str. 3
D72076 Tübingen, Germany
Email: {oezlem.guervit,dkfreude,martin.skalej}@med.uni-tuebingen.de

Abstract. Based on the VIVENDI-framework for virtual endoscopy, we present a system for the interactive and multi-modal representation of important anatomical structures for neuroendoscopic interventions.
A serious problem of neuroendoscopic interventions is the possibility of injuring a blood vessel while performing endoscopic surgery inside the human brain. Besides the sudden loss of optical visibility due to the red-out of the injured vessel, a potential lethal mass bleeding can be the fatal outcome of the intervention. To avoid accidental lesions, we represent the relevant information using multiple volumetric MRI-based representations of the respective organs.
Keywords: Virtual Environments, Magnetic-Resonance-Imaging, MR Angiography, Virtual Neuroendoscopy, Computer Assisted Diagnosis.

1 Introduction

Minimal-invasive neurosurgical procedures are rapidly gaining importance in neurosurgery. Besides the reduced damage of brain tissue compared to commonly used surgical techniques, regions of the brain become accessible, which are not approachable for previous techniques. However, minimal-invasive neurosurgical procedures facilitate only limited access to the respective brain region. In case of a serious complication, such as a mass bleeding after injuring a major blood vessel, effective *stanching* of that injury is usually not possible.

Our focus is on minimal-invasive interventions in the ventricular system of the human brain, where the *cerebrospinal fluid (CSF)* is produced and distributed via the ventricles to the other cavities inside of the skull. Sometimes the cerebral aqueduct – a narrow passage between the third and fourth ventricle – is occluded due to a tumor, an

injury due to an accident, or a native defect, thus blocking the natural flow of the CSF. This blockage leads to a dangerous increase of brain pressure which can damage the brain severely. Other problems include the formation of a CSF-filled cyst which also introduces pressure on blood vessels, nerves, or the ventricular (cerebral) aqueduct.

To avoid these dangerous increases of pressure inside of the skull, the cyst is drained or a *ventriculostomy* is applied, where a new CSF drain is realized in the floor of the third ventricle using endoscopic tools. Unfortunately, the major basilar artery is located directly below the floor of the third ventricle without an optical visibility from the third ventricle. Lesions of these arteries result usually in a fatal outcome of the intervention. Even if only a small blood vessel is injured by one of the endoscopic tools, the sudden loss of optical visibility through the endoscope introduces severe difficulties for obtaining the desired results of the interventions.

To avoid traumas of such blood vessels, we modified the VIVENDI-framework for virtual endoscopy [2, 4] to represent multiple anatomical information of the patient data using several 3D scanning techniques.

In the remaining parts of the paper, we briefly discuss related work in the field of virtual endoscopy in Section 2, introduce the existing VIVENDI-framework and describe the additionally used techniques in Section 3. In Section 4, we discuss the learned lessons and finally, we summarize our paper in Section 5.

2 Related Work

Research on virtual endoscopy is one of the most active areas in virtual medicine. The developed methods have been applied to virtual colonoscopy [10, 16], bronchoscopy [7], ventriculoscopy [1, 3], and angioscopy [6, 5, 8, 4].

Different rendering techniques are used to provide sufficient visual quality and/or interactivity. Standard graphics hardware is used to render surface models [17, 12, 10, 2], extracted with the Marching Cubes algorithm [11]. In contrast, volume-rendering techniques are used, partially for better visual quality, partially for interactive speed [15, 20, 8, 1]. Unfortunately, interactive speed was always compromising visual quality, general applicability, or flexibility. In [15] and [5], key-framed animations are generated offline, which frequently leads to the time-intense refinement of the key-framed animation. You et al. used a 16 processor SGI Challenge for parallel volume-rendering of isosurfaces [20]. In contrast, Gobetti et al. used the 3D texture mapping hardware abilities of high-end graphics systems for volume rendering. However, the lack of shading reduced the visual quality significantly [8][1]. Furthermore, the size of the texture memory limits the size of datasets severely, while swapping techniques like bricking reduce the framerate. The Navigator software of General Electric uses isosurface ray casting with approximately one frame per second. Even if the performance of the 1996 results has significantly improved, it hardly can be viewed as interactive [6].

[1] In 1998, Westermann and Ertl presented 3D texture mapping-based volume-rendering with isosurface shading [19]. However, this approach does not provide sufficient performance for interactive endoscopy applications.

Besides rendering, the used navigation paradigm determines the usability of a virtual endoscopy system. Many systems [12, 5, 16, 13] use a planned or automatic navigation, which generates an offline animation of a fly-through after specifying a camera path. This simple scheme reduces the interaction to a VCR-like functionality, requiring a costly refinement of the camera path (and of the animation), if the structure of interest is not well covered. A variation of the planned navigation is the "reliable navigation" [9], in which a complete "visit" of all structures of the organ is guaranteed. However, this also means that user interaction is limited and that not relevant regions cannot easily be skipped.

A free navigation approach is followed by [6, 7, 1]. Unfortunately, the complexity of the anatomical structures commonly found in the datasets is very high. Even for a specifically trained physician, it can be difficult to navigate to the target. Furthermore, collision avoidance is a costly operation which is frequently not available in these systems. In [10, 2, 4], a guided navigation paradigm was adopted in order to provide full navigation flexibility, combined with user guidance and an efficient collision avoidance scheme.

Considering the pros and cons of these approaches, the VIVENDI-framework adopted a surface rendering approach based on [2] and a guided-navigation approach.

3 The VIVENDI-framework for Virtual Endoscopy

The first step after data acquisition of the volume dataset – based on the image stack from rotational angiography, MRI, or Computed Tomography (CT) –, is the segmentation of the respective organs. Standard 3D region growing-based segmentation algorithms [2] can be used as well as advanced segmentation methods [18]. Subsequently, an octree-hierarchical, MarchingCubes-based isosurface algorithm is applied to extract the isosurface representing the inner surface of the respective organ system. Finally, distance fields are computed to provide a guided-navigation system for the virtual camera [10].

VIVENDI uses the octree-oriented subdivision of the isosurfaces geometry to apply an OpenGL-based view-frustum culling and Hewlett-Packard occlusion culling flag [14] scheme to cull on average 90% of the geometry [2–4], resulting in more than 25 fps on an HP J7000/fx6 graphics workstation, and about 20 fps on an HP X-class PC with a fx6 graphics card running LINUX. The distance fields are employed to implement a collision avoidance system and a guided-navigation scheme, which directs the user to a specified target point, while it still guarantees full navigation flexibility [10]. If a 3D, intra-operative navigation system is present, the position and orientation information of the optical endoscope can be fed into VIVENDI to synchronize the virtual and optical endoscopic exploration throughout the neuroendoscopic intervention[2].

[2] At this point no commercially available navigation system provides this information to an external entity. VIVENDI however, can process information of this kind.

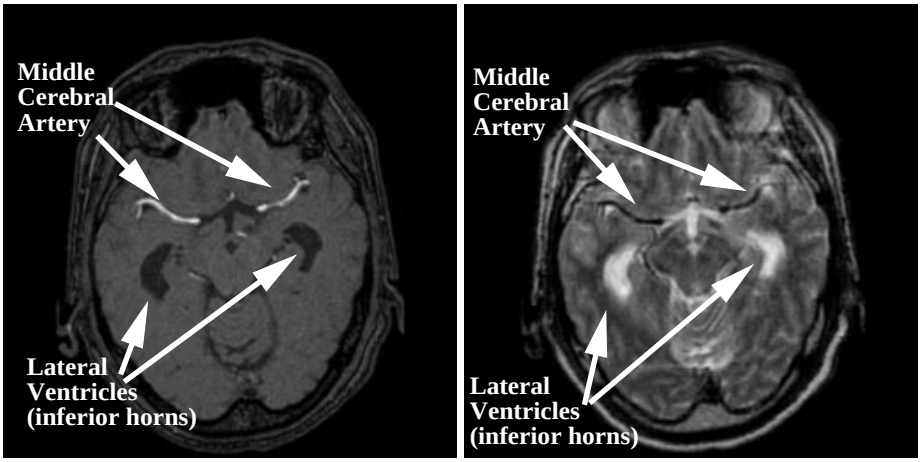

(a) (b)

Fig. 1. MRI axial slice with the inferior horns of the lateral ventricles and middle cerebral artery (left and right). (a) MRI Angiography sequence, (b) MRI TSE sequence.

Based on techniques developed for combining multiple target points for guided-navigation and disconnected anatomical structures [2], we integrate the concurrent rendering of information from two data modalities. We use an MRI TSE (Turbo Spin Echo) sequence to generate the inner surface of the CSF-filled cavities (Fig. 1b) – such as the ventricular system or cysts –, and an MRI Angiography (Time of Flight sequence) to derive information on the vascular system (Fig. 1a) in the area of interest. Both sequences were performed subsequently, without changing the position and orientation of the patient. It later turned out in our experiments that patient movement during both scans is negligible. Although the resolution within the axial slices is twice as large in the MRI Angiography as in the MRI TSE sequence, the scans generate two well-aligned data volumes. However, the number of axial slices in the MRI data is different, and hence so is the covered scanning area. This difference requires a manual slice matching step that is performed by a neuroradiologist or neurosurgeon. The resulting axial translation generates an error which is at most the distance between two slices in the data volumes. A manifestation of this error can be found in Figures 3 and 4 (see Appendix), where the red/dark artery geometry reconstructed from the MRI Angiography sequence penetrates the geometry of the transparent CSF-filled cavity geometry[3]. Especially in Figure 4 (see Appendix), the "original" position of the blood vessel is also visible in the geometry extracted from MRI TSE sequence. Fortunately, the maximum error (if the matching step is correct) is always sufficiently below a critical threshold, where the "clearance area" would also cover the proposed target area of the endoscope.

[3] The depth sorting of the geometry for correct transparent rendering is obtained by the view-frustum culling. All subdivision entities are sorted according to their closest depth values.

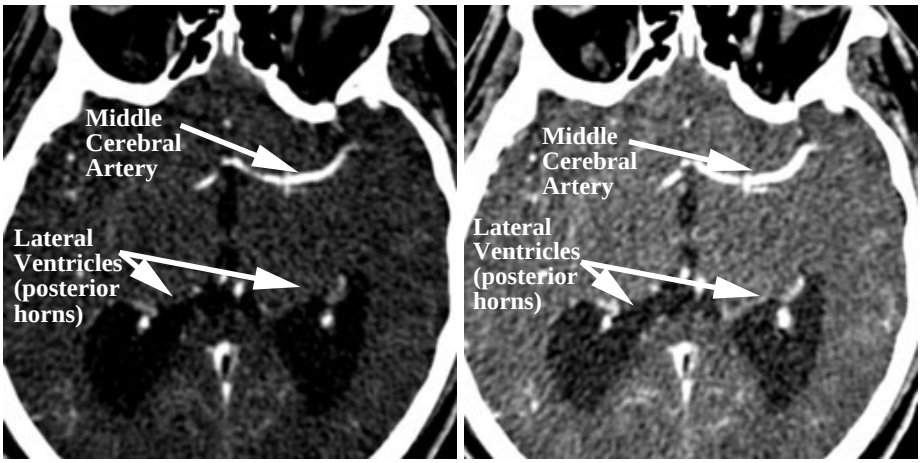

(a) (b)

Fig. 2. CT axial slice with the posterior horns of the lateral ventricles and middle cerebral artery. (a) Contrast window one, (b) Contrast window two.

4 Lessons Learned

We applied our methods to a set of different patient datasets. Most patients received a ventriculostomy to treat the aqueductal stenosis (see Figures 6 and 5 in Appendix). Two other patients suffered from a large cyst in the third ventricle and near the left temporal lobe (see Figs. 3 and 4 in Appendix) and were treated with a drainage of the cyst. As mentioned earlier, the neurosurgeons performed these interventions using minimal-invasive procedures that introduce a non-negligible risk of damaging a major artery close to the new drain.

We conducted several experiments to determine an appropriate scanning protocol which produces volume datasets which can be matched using CT- and MRI scanners. For this purpose, two anatomical structures need to be identified by the scanning procedure; the CSF-filled ventricular system and cysts, and the blood filled major arterial blood vessels in proximity to the CSF-filled target areas.

The (contrast agent-enhanced) CT scan provided a good contrast and a high resolution for the vascular system within the region of interest. However, this sequence did not produce a sufficient contrast between the brain tissue and the CSF-filled cavities, while still preserving the complete inner surface of the cavities (Fig. 2a/b). Furthermore, Computed Tomography inherently introduces radiation, an additional drawback compared to MRI.

Blood-flow induced MRI Angiography (Fig. 1a) also reconstructs the vascular system with good quality, although the resolution is slightly lower than with a CT scan. However, it is not usable for the segmentation of CSF-filled cavities. Therefore, we perform a second sequence that focuses on these cavities right after the MRI Angiography.

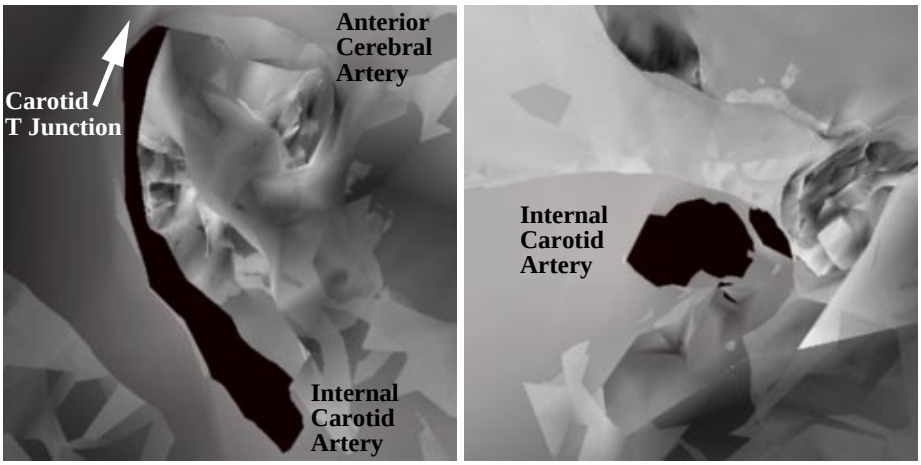

(a) (b)

Fig. 3. (a) Close-up to internal carotid artery, (b) View downwards on the "carotid siphon", below the carotid T junction.

We previously used an MRI 3D CISS (Constructive Interference in Steady States) sequence to reconstruct the ventricular system in patient datasets. Unfortunately, the different scanning orientation (sagittal and axial) introduced a surprisingly difficult match procedure, which qualified this sequence as impractical. Consequently, we modified the 3D CISS sequence to an MRI TSE sequence (Fig. 1b) which provides the same orientation as the angiography sequence and unfortunately, also a smaller slice range than the 3D CISS. However, it turned out that the resolution is sufficient for our purposes. Finally, the combination of angiography and MRI TSE data delivered a satisfying matching and image quality and was henceforth used in all later experiments. Furthermore, MRI does not expose radiation, in contrast to a CT scan.

The current system is now providing the vascular topography combined with the (already previously available) information of the anatomical structure of the CSF-filled ventricular cavities. This information is successfully used to represent the location of the blood vessels to carefully plan the neuroendoscopic intervention. Lesions of the respective arteries can be avoided, resulting in a substantial reduction of the risk of serious complications. Up to now, five patients were scanned using the described protocol and provided a useful planning aid for the neuroendoscopic interventions.

5 Conclusion

In this paper, we presented a virtual neuroendoscopy system, based on the VIVENDI framework for virtual endoscopy. Interactive performance on a graphics workstation (or PCs) and intuitive handling was achieved using a visibility driven rendering and by adopting the guided-navigation paradigm.

A reliable MRI-based scanning protocol was established which provides the necessary information for the successful planning of neuroendoscopic procedures which significantly reduce the risk of serious complications. Note that the problems described in this paper are not strictly specific to neuroendoscopy, but are also present in other medical application fields, such as oral-maxillofacial or cardio-thoracic surgery, which will be the focus of future work.

Acknowledgments

This work has been supported by the Hewlett-Packard Workstation System Lab, Ft. Collins, USA, by the Ministry of Science, Research, and Arts of the State of Baden-Württemberg, and by the Deutsche Telekom AG. Datasets were provided by the Department of Neuroradiology. Especially, we would like to thank Sabine Joachim, Violeta Adis, and Bernd Kardatzki of the Department of Neuroradiology for their help obtaining and transferring the various patient datasets, and Mike Doggett for proof-reading.

References

1. D. Auer and L. Auer. Virtual Endoscopy - A New Tool for Teaching and Training in Neuroimaging. *International Journal of Neuroradiology*, 4:3–14, 1998.
2. D. Bartz and M. Skalej. VIVENDI - A Virtual Ventricle Endoscopy System for Virtual Medicine. In *Proc. of Symposium on Visualization*, pages 155–166,324, 1999.
3. D. Bartz, M. Skalej, D. Welte, W. Straßer, and F. Duffner. A Virtual Endoscopy System for the Planning of Endoscopic Interventions in the Ventricle System of the Human Brain. In *Proc. of BiOS'99: Biomedical Diagnostics, Guidance and Surgical Assist Systems*, volume 3514, pages 91–100, 1999.
4. D. Bartz, W. Straßer, M. Skalej, and D. Welte. Interactive Exploration of Extra- and Intracranial Blood Vessels. In *Proc. of IEEE Visualization*, pages 389–392,547, 1999.
5. J. Beier, T. Diebold, H. Vehse, G. Biamino, E. Fleck, and R. Felix. Virtual Endoscopy in the Assessment of Implanted Aortic Stents. In *Proc. of Computer Assisted Radiology*, pages 183–188, 1997.
6. C. Davis, M. Ladds, B. Romanowski, S. Wildermuth, J. Knoplioch, and J. Debatin. Human Aorta: Preliminary Results with Virtual Endoscopy Based on Three-dimensional MR Imaging Data Sets. *Radiology*, 199:37–40, 1996.
7. G. Ferretti, D. Vining, J. Knoplioch, and M. Coulomb. Tracheobronchial Tree: Three-Dimensional Spiral CT with Bronchoscopic Perspective. *Journal of Computer Assisted Tomography*, 20(5):777–781, 1996.
8. E. Gobbetti, P. Pili, A. Zorcolo, and M. Tuveri. Interactive Virtual Angioscopy. In *Proc. of IEEE Visualization*, pages 435–438, 1998.
9. T. He and L. Hong. Reliable Navigation for Virtual Endoscopy. In *Proc. of IEEE Medical Imaging*, 1999.
10. L. Hong, S. Muraki, A. Kaufman, D. Bartz, and T. He. Virtual Voyage: Interactive Navigation in the Human Colon. In *Proc. of ACM SIGGRAPH*, pages 27–34, 1997.
11. W. Lorensen and H. Cline. Marching Cubes: A High Resolution 3D Surface Construction Algorithm. In *Proc. of ACM SIGGRAPH*, pages 163–169, 1987.

12. W. Lorensen, F. Jolesz, and R. Kikinis. The Exploration of Cross-Sectional Data with a Virtual Endoscope. In R. Satava and K. Morgan, editors, *Interactive Technology and New Medical Paradigms for Health Care*, pages 221–230. 1995.
13. G. Rubin, C. Beaulieu, V. Argiro, H. Ringl, A. Norbash, J. Feller, M. Dake, R. Jeffrey, and S. Napel. Perspective Volume Rendering of CT and MR Images: Application for Endoscopic Imaging. In *Radiology*, volume 199, pages 321–330, 1994.
14. N. Scott, D. Olsen, and E. Gannett. An Overview of the VISUALIZE fx Graphics Accelerator Hardware. *The Hewlett-Packard Journal*, (May):28–34, 1998.
15. R. Shadidi, V. Argiro, S. Napel, L. Gray, H. McAdams, G. Rubin, C. Beaulieu, R. Jeffrey, and A. Johnson. Assessment of Several Virtual Endoscopy Techniques Using Computed Tomography and Perspective Volume Rendering. In *Proc. of Visualization in Biomedical Computing*, volume LNCS 1131, pages 521–528, 1996.
16. D. Vining, R. Shifrin, E. Grishaw, K. Liu, and R. Choplin. Virtual Colonoscopy (abstract). In *Radiology*, volume 193(P), page 446, 1994.
17. D. Vining, D. Stelts, D. Ahn, P. Hemler, Y. Ge, G. Hunt, C. Siege, D. McCorquodale, M. Sarojak, and G. Ferretti. FreeFlight: A Virtual Endoscopy System. In *First Joint Conference, Computer Vision, Virtual Reality and Robotics in Medicine and Medical Robotics and Computer-Assisted Surgery*, volume LNCS 1205, pages 413–416, 1997.
18. D. Welte and U. Klose. Segmentation and Selective Imaging of Arteries and Veins from Contrast-Enhanced MRA Data. In *Proc. of European Congress of Radiology*, 1999.
19. R. Westermann and T. Ertl. Efficiently Using Graphics Hardware in Volume Rendering Applications. In *Proc. of ACM SIGGRAPH*, pages 169–177, 1998.
20. S. You, L. Hong, M. Wan, K. Junyapreasert, A. Kaufman, S. Muraki, Y. Zhou, M. Wax, and Z. Liang. Interactive Volume Rendering for Virtual Colonoscopy. In *Proc. of IEEE Visualization*, pages 343–346, 1997.

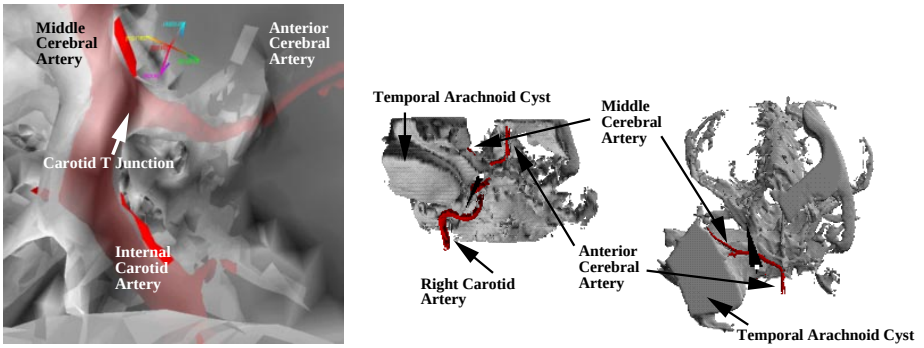

(a) (b)

Fig. 4. Temporal Arachnoid Cyst dataset: (a) View on to carotid T junction, where the internal carotid artery branches into the lateral middle cerebral artery and the frontal anterior cerebral artery. The red vascular geometry – extracted from MRI Angiography – penetrates through the visible vascular geometry extracted from MRI TSE. (b) Frontal and top overview of temporal arachnoid cyst.

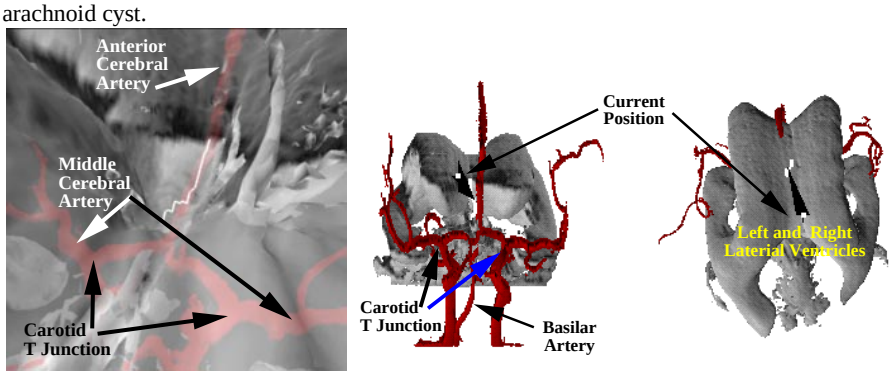

(a) (b)

Fig. 5. Ventriculostomy dataset: (a) Frontal view from the center of the lateral ventricles (first two ventricles); the septum between the lateral ventricles is dissolved. The white line marks the default camera path from the left lateral ventricle through the foramen of Monro into the third ventricle. (b) Frontal and top overview of ventricular system.

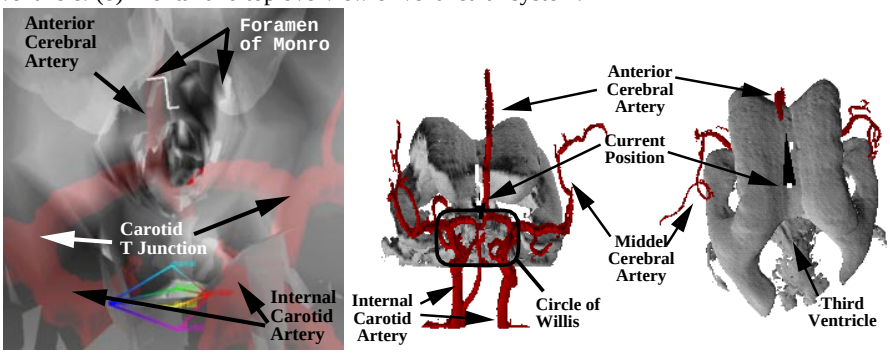

(a) (b)

Fig. 6. Ventriculostomy dataset: (a) Frontal view from the cerebral aqueduct entrance in the third ventricle. The floor of the third ventricle – the potential location for a new CSF drain – is bounded by the arterial *circle of Willis*, a potential cause for mass bleeding. (b) Frontal and top overview of ventricular system.